



Effects of Temperature and Heat Input on the Wear Mechanisms of Contact Tube for Non-copper-Coated Solid Wires

Zhuoxin Li, Qian Wan, Tao Yuan, Tianli Zhang, Guodong Li, and Hong Li

(Submitted July 15, 2018; in revised form April 8, 2019; published online May 13, 2019)

Contact tube wear is the bottleneck of industrial application for non-copper-coated solid wire. It is crucial that we understand the wear mechanism of contact tube so that we can decrease contact tube wear. The effects of temperature and heat input on contact tube wear were investigated in this work. The results demonstrated that fatigue peeling was the main wear mechanism of the contact tube at room temperature without supplying a welding current. Adhesive wear, oxidative wear and abrasive wear were the primary wear mechanisms of the contact tube at 450 °C without supplying a welding current. The wear rate of the contact tube during welding was significantly enhanced in comparison with the wear rate at 20 °C and 450 °C. The effect of contact tube temperature on the wear properties of the contact tube was limited. The wear rate of the contact tube was increased with increasing heat input for non-copper-coated solid wire. The wear mechanism of the contact tube was converted from oxidative wear to arc ablation at the heat input of 9114 J/cm.

Keywords contact tube, heat input, joining, non-copper-coated solid wire, steel, wear mechanism

1. Introduction

Environmentally friendly non-copper-coated solid wires have the potential application in robotic arc welding. However, the contact tube wear limits the wide industrial application of non-copper-coated solid wires (Ref 1). The wear properties of the contact tube significantly influence the alignability and feedability of welding wires. The contact tube wear evidently reduces the precision of trajectory planning and seam tracking for welding robots (Ref 2, 3). Various factors synthetically affect the wear properties of the contact tube. These factors include the lubricating properties of coatings, the contact tube temperature, the heat radiation from arc and molten pool, the welding current and the mechanical friction heat. In general, the contact tube temperature is derived from the synergistic effect of various factors during welding. The heat input essentially represents the effect of welding current, arc voltage and the welding speed (Ref 4). In summary, the contact tube temperature and heat input are critical factors in influencing the wear properties of contact tube for non-copper-coated solid wires.

Zhuoxin Li, Qian Wan, Guodong Li, and Hong Li, College of Materials Science and Engineering, Beijing University of Technology, 100 Ping Le Yuan, Chaoyang District, Beijing 100124, China; **Tao Yuan**, College of Mechanical Engineering and Applied Electronics Technology, Beijing University of Technology, 100 Ping Le Yuan, Chaoyang District, Beijing 100124, China; and **Tianli Zhang**, School of Materials Engineering, Shanghai University of Engineering Science, 333 Longteng Road, Songjiang District, Shanghai 201620, China. Contact e-mail: 2223508501@qq.com.

Temperature plays an important role in the wear of contact tube. When copper plating solid wires were welded for 30 min, the contact tube temperature reached approximately 407 °C at a distance of 2 mm from the tip, whereas the temperature reached approximately 447 °C for non-copper-coated solid wires at the same welding time. The temperature difference is caused by the difference of the Joule heat generated at the sliding contact (Ref 5). When the radiative heat from the arc and molten pool was shielded, the contact tube temperature reached approximately 227 °C at the welding time of 220 s. When the contact tube was affected by the radiative heat from the arc and molten pool, the contact tube temperature reached approximately 327 °C over the same time (Ref 6). It was reported that the contact tube temperature reached approximately 400 °C at points 10 mm from the tip when welding for 150 s (Ref 7). Adam et al. observed that the contact tube temperature reached approximately 480 °C with an air-cooled gun when welding for 100 s. The major sources of contact tube heating are radiation from the arc and resistive heating from the electrode–contact tube interface (Ref 8). It is important to understand the wear mechanisms of contact tube under different temperatures.

The tribological behaviors of the contact tube are investigated by friction and wear experiment instruments for low-carbon steels against pure copper or copper alloys pairs. These results provide some information about the wear mechanisms of contact tube. The friction coefficient of borided bearing steels decreased with an increase in the temperature from room temperature to 600 °C. In this case, the wear rates increased as the temperature was raised (Ref 9). The dominant wear mechanisms of copper are brittle fracture and delamination wear at low temperatures (up to 300 °C), whereas oxidative mild wear occurs at high temperatures (greater than 300 °C). The wear mode of pure copper changes from oxidative to abrasive wear or arc ablation as the electrical current intensity increases (Ref 10). The wear rate of both Cu-Cr-Zr and Cu-Cr-Ag copper alloys increased with increasing electrical current. Adhesive wear, abrasive wear and arc erosion are the primary

mechanisms of copper alloy wear during the electrical sliding processes (Ref 11-13). With the transition of the contact tube wear from mild to severe, the dominant wear mechanisms of contact tube change from fatigue peeling and oxidative wear to abrasive wear and arc ablation (Ref 14). However, the operational conditions of these tribological instruments are different from the conditions to which the contact tube is exposed during welding. During welding, the contact tube is continuously influenced by the welding current of 300 A, the high temperature of 380-450 °C, the shielding gas and the heat radiating from arc and the molten pool. The tribological test results are not suitable for controlling contact tube wear with these experiment instruments. Therefore, it is necessary to evaluate the wear properties of contact tube with novel test methods.

In this work, we propose a novel friction and wear test method. The wear properties of contact tube were evaluated at room temperature and 450 °C. The effect of heat input on the wear properties of the contact tube was investigated. A contact tube wear map was established. The wear map qualitatively expresses the correlations between the contact tube wear mechanisms, the contact tube temperature and the welding current. The wear map also provides theoretical guidance for the reduction in contact tube wear.

2. Experimental Procedure

2.1 Materials

Two non-copper-coated solid wires (wires A and B) and a commercial copper plating solid wire (wire C) were selected as the welding consumables. The diameter of the solid wire was $\phi 1.2$ mm. The substrate of the solid wire was ER70S-6. All of the solid wires conformed to AWS A5. 18 M: 2005. The surface coating compositions of the solid wires are shown in Table 1. A Cr-Zr-Cu contact tube measured approximately $\phi 1.36$ mm in inner diameter. The chemical composition of the contact tube is shown in Table 2.

2.2 Measurement of Contact Tube Temperature

A circular groove was machined at a point 3 mm from the contact tube tip. A thermocouple was placed in the circular groove to measure the contact tube temperature. As illustrated

in Fig. 1, the contact tube temperature was continuously recorded through the temperature recorder. The contact tube temperature was measured for a welding period of 300 s. The welding conditions are shown in Table 3.

2.3 Wear Properties of Contact Tube Testing

As shown in Table 3, the cold test method is described as following. The contact tube was held at room temperature. The welding wire was continuously moved along the inner surface of the contact tube for 3 h. The feeding speed of the welding wire was 12 m/min. Under the cold test conditions, the wear properties of the contact tube were tested with an automatic wire feeder, as described in Fig. 2(a). The wear properties of the contact tube at room temperature were defined as the cold wear properties of the contact tube.

Similarly, the hot test conditions shown in Table 3 are depicted as follows. The contact tube was placed in an electric furnace, where temperature was held at 450 °C. The welding wire was continuously moved with the speed of 12 m/min for 3 h. The wear properties of the contact tube were tested with an automatic wire feeder, as depicted in Fig. 2(b). The wear properties of the contact tube at 450 °C were identified as the hot wear properties of the contact tube.

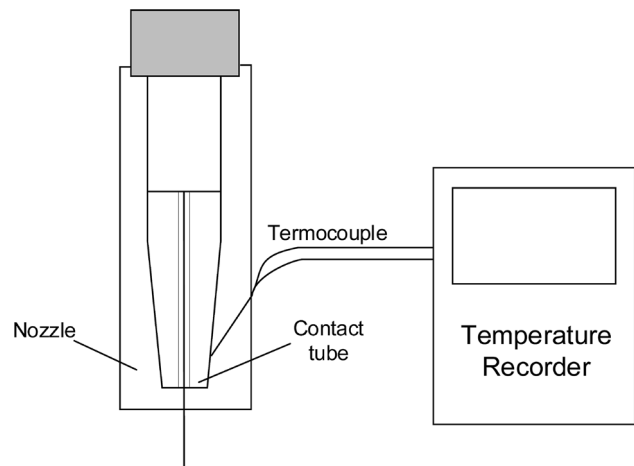


Fig. 1 Scheme of measurement devices of contact tube temperature for wire A, wire B and wire C

Table 1 Surface coatings compositions of wire A, wire B and wire C

Number of solid wires	Compositions of main solid lubricants, wt.%			
	C	MoS ₂	Fe ₃ O ₄	Fe ₂ O ₃
A	37.5	25	37.5	0
B	50	0	0	50
C	Copper plating			

Table 2 Chemical composition of Cr-Zr-Cu contact tube

Element	Al	Mg	Cr	Zr	Fe	Si	P	Impurity	Cu
Content	0.1-0.25	0.1-0.25	0.4-0.8	0.3-0.8	0.05	0.05	0.01	0.5	Bal.

Table 3 Cold wear conditions, hot wear conditions and welding conditions of the contact tube for wire A, wire B, and wire C

Test parameters	Cold wear conditions	Hot wear conditions	Welding conditions
Current/voltage			280-320 A/33-36 V
Welding speed, cm·min ⁻¹			45
Extension length, mm			20
Polarity			Direct current electrode positive (DCEP)
Test temperature, °C	20	450	Obtained from thermocouple
Feeding time of wire, h	3		
Wire feed speed, m·min ⁻¹	12		
Shielding gas and flow rate	100% CO ₂ , 20 L/min		

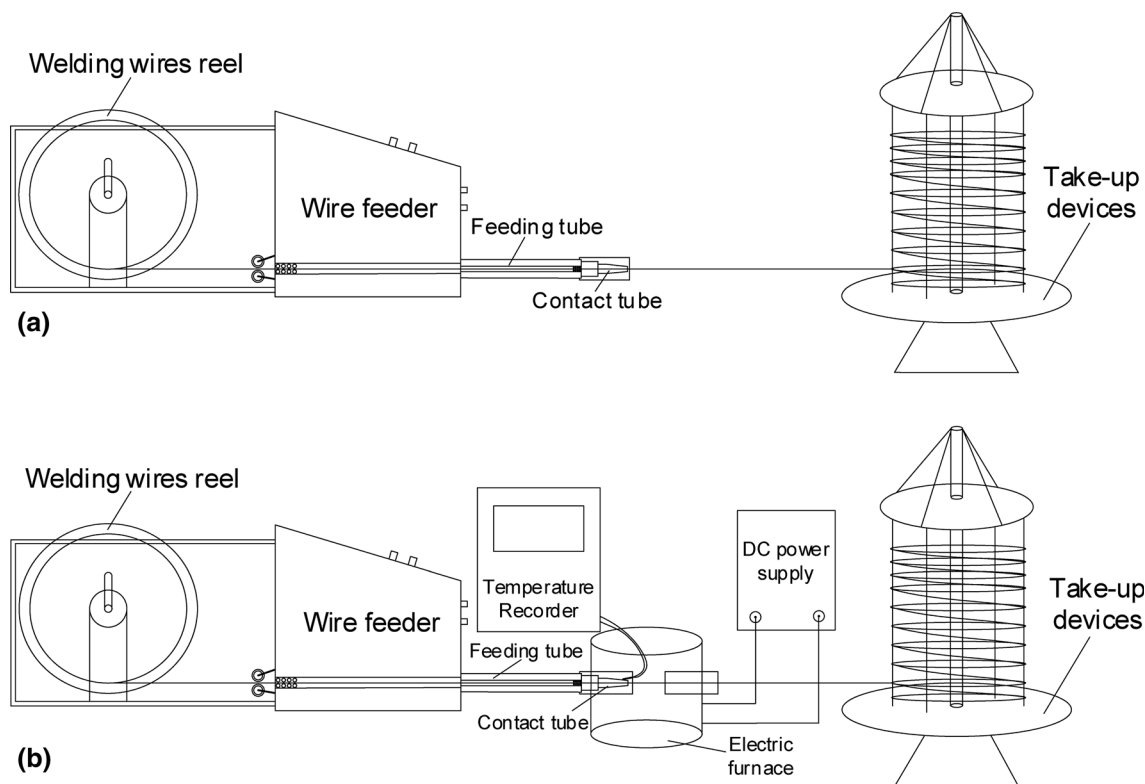


Fig. 2 Sketch of test devices of (a) cold wear properties of contact tube, (b) hot wear properties of contact tube. Test conditions: $T =$ (a) 20 °C or (b) 450 °C, feeding time of wire = 3 h, feed speed of wire = 12 m/min, flow rate of 100% CO₂ shielding gas = 20 L/min

A MOTOMAN welding robot was used as the auto-welding equipment. The power source was a MOTOWELD-S350 welding machine (SG-MOTOMAN). The contact tube was fixed during welding. The welding wire was fed with the sliding velocity of 12 m/min for 3 h. The welding conditions are exhibited in Table 3. The wear properties of the contact tube were evaluated under the welding conditions.

Based on the welding parameters in Table 4, the wear properties of the contact tube for wire A were tested at the heat inputs of 4200, 6072, 9114 and 11,760 J/cm, respectively, corresponding to welding currents of 150, 220, 280 and 350 A. The heat input was calculated according to formula 1.

$$E = \frac{\eta UI}{v} \quad (\text{Eq 1})$$

where E is the heat input, η is the heat efficiency where for gas shielded arc welding, $\eta = 0.7$, U is the arc voltage, I is the welding current and v is the welding speed.

2.4 Characterization

Before each test, to remove surface contaminants, each contact tube was placed into an acetone solution with ultrasonic cleaning for 20 min. The contact tube was then dried out and weighed with an analytical balance, the precision of which was 0.0001 g. The initial weight of the contact tube was denoted as m_0 . The initial inner diameter of the contact tube was determined by an OLYMPUS SZ61-type stereoscopic microscope, with the value denoted as D_0 . After welding, spatter and pollutants on the surface of the contact tube were removed. Then, the contact tube was ultrasonically cleaned for another

Table 4 Welding parameters of the wire A

Current/voltage	Welding speed, cm min ⁻¹	Heat input, J/cm	Shielding gas	Gas flow rate, L min ⁻¹	Extension length, mm	Polarity	Welding time, h
150A/20 V	30	4200	100%CO ₂	20	20	DCEP	1
220A/23 V	35	6072					
280A/31 V	40	9114					
350A/36 V	45	11,760					

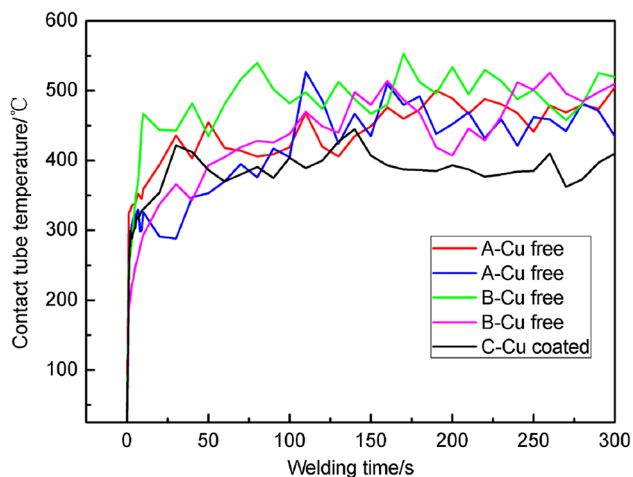


Fig. 3 Contact tube temperature trends for wire A, wire B and wire C during welding. Test conditions: $I = 280\text{--}320$ A, $U = 33\text{--}36$ V, welding speed = 45 cm/min, extension length of wire = 20 mm, DCEP, welding time = 300 s, feed speed of wire = 12 m/min, flow rate of 100% CO₂ shielding gas = 20 L/min

20 min and dried out. Its postwelding mass was weighed as m_1 with the analytical balance. The maximum inner diameter of the contact tube was determined as D_{\max} by the stereoscopic microscope. In these tests, two parameters must be defined to characterize the wear properties of the contact tube. These parameters are the mass loss rate of the contact tube and the wear rate of the contact tube's inner diameter. The mass loss rate of the contact tube (m_{wear}) and the wear rate of the contact tube's inner diameter (D_{wear}) were calculated according to formulas 2 and 3.

$$m_{\text{wear}} = \frac{m_0 - m_1}{m_0} \times 100\% \quad (\text{Eq 2})$$

$$D_{\text{wear}} = \frac{D_{\max} - D_0}{D_0} \times 100\% \quad (\text{Eq 3})$$

The contact tube was cut into two identical parts along the radial direction with a wire-cut electric discharge machine. Then, the half contact tube was cut into a 15 mm × φ10 mm segment along its transverse direction. The cut location was close to the contact tube tip. The contact tube sample was then cleaned with acetone to remove all surface contaminants. Worn surfaces of the contact tube were investigated using scanning

electron microscope (SEM, FEI Quanta 200F) and an energy-dispersive x-ray spectroscopy (EDS).

3. Experimental Results

3.1 Wear Properties of the Contact Tube under Different Test Conditions

Figure 3 shows the contact tube temperature trends during welding. The contact tube temperature increased to approximately 300 °C at 25 s. The contact tube temperature fluctuated at 380–510 °C with welding time. These differences of the contact tube temperature are caused by electrical contact resistances between the welding wire and the contact tube (Ref 15). The average contact tube temperatures were approximately 460 °C, 500 °C, and 380 °C for wires A, B, and C, respectively.

The hot wear rate of the contact tube is slightly higher than its cold wear rate, as presented in Fig. 4, so temperature does influence the wear properties of the contact tube. It was observed that the contact tube of wire A had the lowest wear rate, followed by that of wire B and finally, where the contact tube of wire C had the highest wear rate. Figure 5 shows the wear properties of contact tube under different test conditions. These test conditions included the cold wear conditions, the hot wear conditions and the welding conditions. It was found that the wear rate of the contact tube during welding is significantly higher than its cold wear rate and hot wear rate. Therefore, welding plays a critical role in influencing the wear properties of contact tube.

According to Fig. 6, the wear rate of the contact tube increases with the increase in heat input. The effect of heat input on the wear properties of the contact tube indicates a transition point. A transition from mild to severe contact tube wear was clearly observed in the worn morphology of the contact tube. When the heat input was less than 9114 J/cm, the gradient of the wear rate of the contact tube was lower, whereas the contact tube wear was mild. When the heat input was greater than 9114 J/cm, the gradient of the wear rate of the contact tube was significantly higher. In this case, the contact tube suffered a transition from mild to severe wear.

3.2 Worn Morphology of the Contact Tube under Different Wear Conditions

Table 5 shows the cold worn morphology of the contact tube and interface compositions. The worn surface of the contact tube for wire A was smoother. The surface was covered

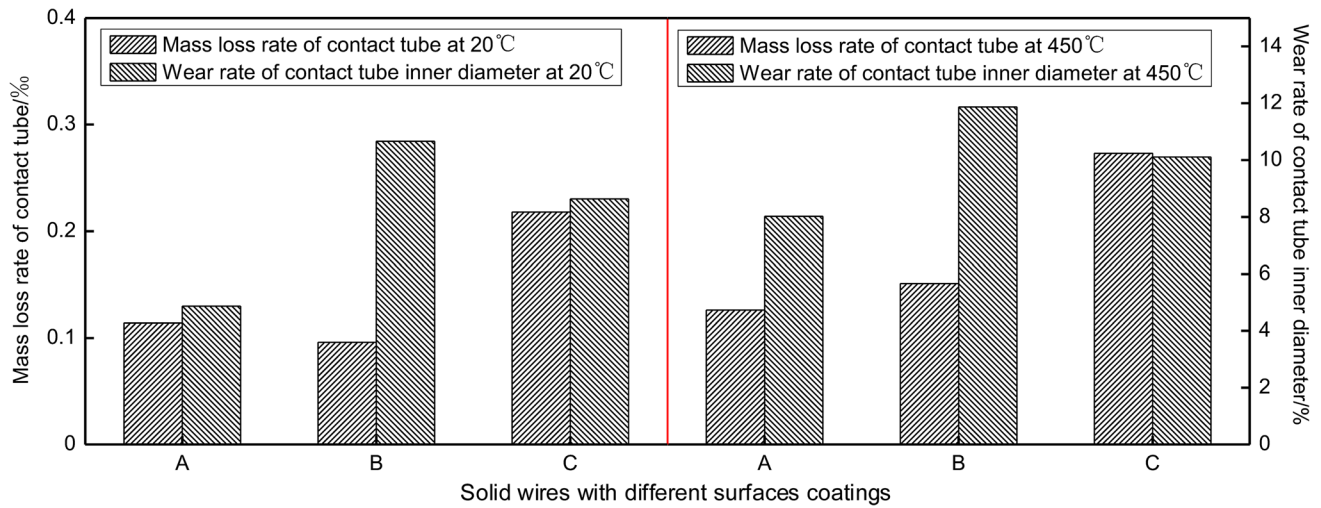


Fig. 4 Wear properties of the contact tube for wire A, wire B and wire C at 20 °C and 450 °C. Test conditions: $T = 20\text{ °C}$ or 450 °C , feeding time of wire = 3 h, feed speed of wire = 12 m/min, flow rate of 100% CO₂ shielding gas = 20 L/min

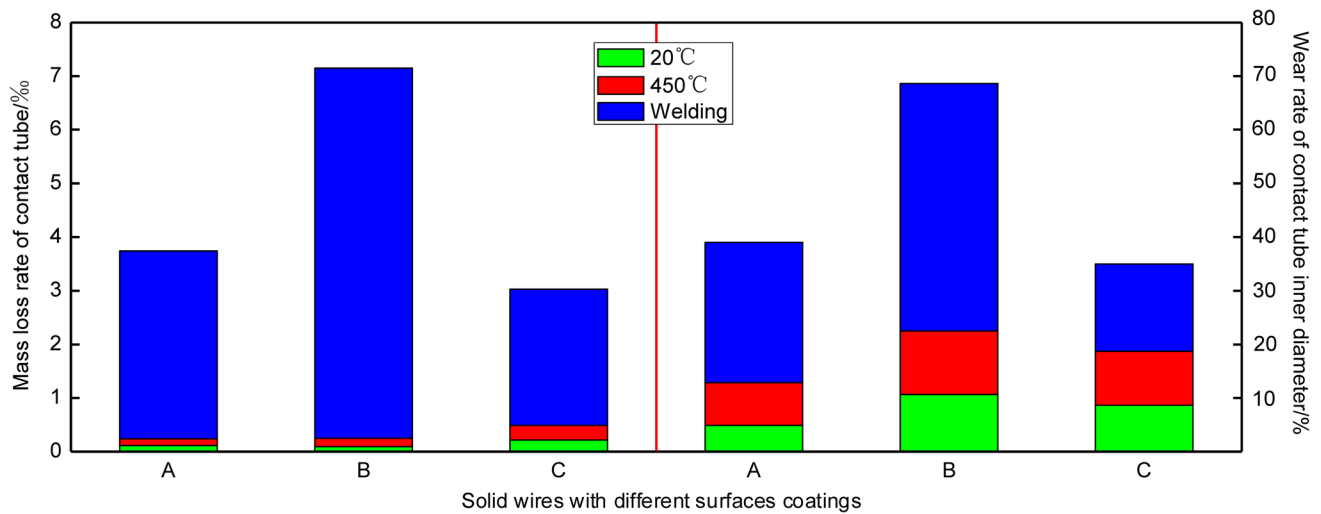


Fig. 5 Wear properties of the contact tube for wire A, wire B and wire C under different conditions: cold wear test, hot wear test, the welding

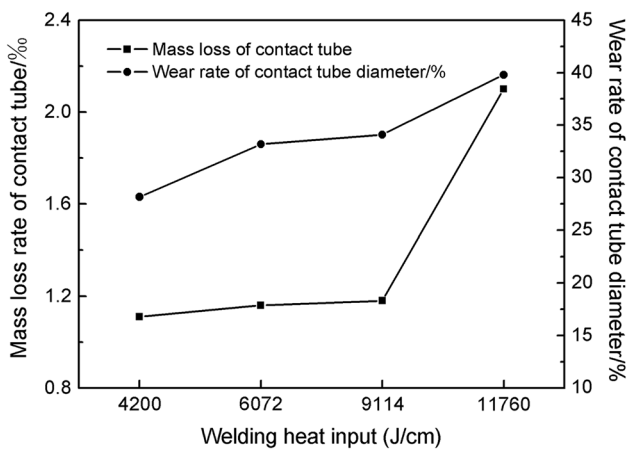


Fig. 6 Wear properties of contact tube for wire A, wire B and wire C under different heat inputs. Test conditions: $I = 150\text{--}350\text{ A}$, $U = 20\text{--}36\text{ V}$, welding speed = 30–45 cm/min, extension length of wire = 20 mm, DCEP, welding time = 1 h, flow rate of 100% CO₂ shielding gas = 20 L/min

with several debris. Lots of debris were distributed at the worn surface of the contact tube for wire C. Some microcracks existed within the bulk materials, demonstrating the typical features of fatigue peeling. The EDS results showed that these debris were composed of the copper element, because the debris peels off from the copper matrix.

Table 6 shows the hot worn morphology of the contact tube and interface compositions. The worn surface of the contact tube for wire A was very smooth. Bulks and little copper debris were found on the surface. The inner surface of the contact tube for wire A was covered with graphite and iron oxides. The inner surface of the contact tube for wire B had numerous deep furrows and debris but less uniformity. The residual quantity of graphite in the grooves was low. Lots of shallow furrows existed at the inner surface of the contact tube for wire C. The EDS analysis of these grooves showed elemental traces of Cu, C and O. The compositions were C, Cu, Fe and O at the smooth zones of the contact tube.

As displayed in Table 7, the inner surface of the contact tube for wire A was smooth. Bulk or granular substances were distributed at the inner surfaces. Debris and adhesive bulks

Table 5 Cold worn morphology of the contact tube and interface compositions for wire A and wire C. Test conditions: $T = 20\text{ }^{\circ}\text{C}$, feeding time of wire = 3 h, feed speed of wire = 12 m/min, flow rate of 100% CO_2 shielding gas = 20 L/min

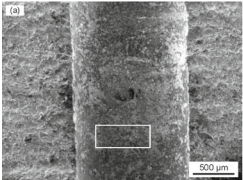
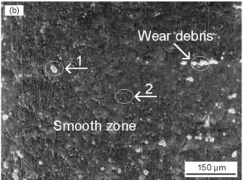
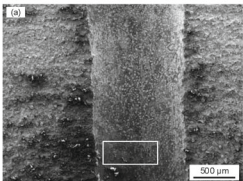
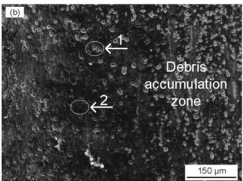
Wires type	Worn morphology of the contact tube		Microzones compositions of the contact tube	
	Macroscopic worn morphology	Microscopic worn morphology	Point 1 composition	Point 2 composition
Wire A			(c) EDS 1 Cu: 86.6 C: 9.2 O: 3.7 Cr: 0.5 (wt.%)	(d) EDS 2 Cu: 64.6 C: 20.2 O: 14.0 Cr: 0.8 Fe: 0.4 (wt.%)
Wire C			(c) EDS 1 Cu: 92.5 C: 1.8 O: 4.2 Cr: 1.0 Fe: 0.4 (wt.%)	(d) EDS 2 Cu: 71.7 C: 12.5 O: 10.8 Cr: 1.0 Fe: 3.6 S: 0.5 (wt.%)

Table 6 Hot worn morphology of the contact tube and interface compositions for wire A, wire B and wire C. Test conditions: $T = 450\text{ }^{\circ}\text{C}$, feeding time of wire = 3 h, feed speed of wire = 12 m/min, flow rate of 100% CO_2 shielding gas = 20 L/min

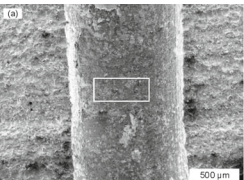
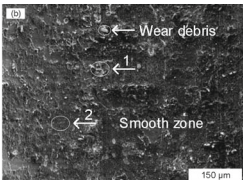
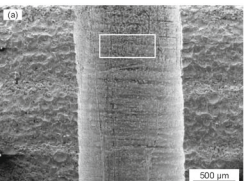
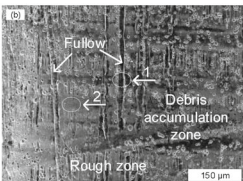
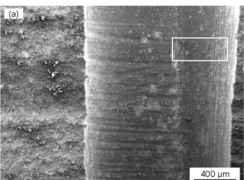
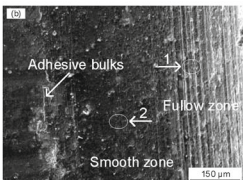
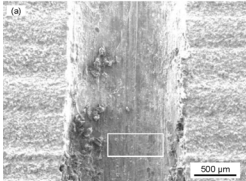
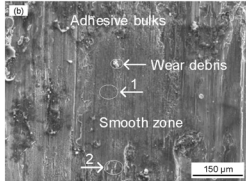
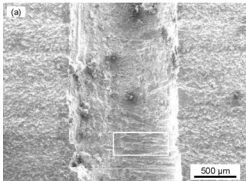
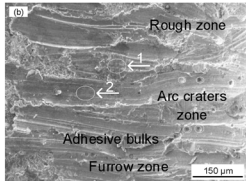
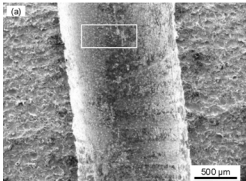
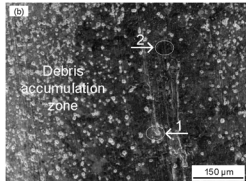
Wires type	Worn morphology of the contact tube		Microzones compositions of the contact tube	
	Macroscopic worn morphology	Microscopic worn morphology	Point 1 composition	Point 2 composition
Wire A			(c) EDS 1 Cu: 85.5 C: 7.7 O: 4.3 Cr: 0.9 Fe: 1.7 (wt.%)	(d) EDS 2 Fe: 35.6 C: 23.5 Cu: 20.3 O: 19.8 S: 0.8 (wt.%)
Wire B			(c) EDS 1 Cu: 88.6 C: 7.8 O: 3.0 Cr: 0.6 (wt.%)	(d) EDS 2 Cu: 81.6 C: 11.1 O: 6.9 Cr: 0.4 (wt.%)
Wire C			(c) EDS 1 Cu: 63.5 C: 25.2 O: 10.2 Fe: 0.8 Cr: 0.2 (wt.%)	(d) EDS 2 C: 38.6 Cu: 32.6 O: 26.4 Fe: 1.6 S: 0.5 Cr: 0.3 (wt.%)

Table 7 Worn morphology of the contact tube and interface compositions for wire A, wire B and wire C during welding. Test conditions: $I = 280\text{--}320$ A, $U = 33\text{--}36$ V, welding speed = 45 cm/min, extension length of wire = 20 mm, DCEP, feeding time of wire = 3 h, feed speed of wire = 12 m/min, flow rate of 100% CO_2 shielding gas = 20 L/min

Wires type	Worn morphology of the contact tube		Microzones compositions of the contact tube	
	Macroscopic worn morphology	Microscopic worn morphology	Point 1 composition	Point 2 composition
Wire A				
Wire B				
Wire C				

were present on the worn surface of the contact tube for wire A. The EDS results showed that the bulk portions were composed of iron oxides. The worn surface of the contact tube for wire B was rough. The inner surface of the contact tube was covered with various furrows. The compositions of these furrows were Cu, O and Fe. Lots of debris were present on the worn surface of the contact tube for wire C. The EDS results showed that the debris was composed of Cu and O. This debris was attributed to the oxidative wear of the contact tube.

3.3 Worn Morphology of the Contact Tube under Different Heat Inputs

Table 8 shows the worn morphology of the contact tube and interface compositions under different heat inputs. It was found that graphite, CuO and iron oxides were present at the smooth zones of the contact tube. When the heat input was 4200 J/cm, most of the inner surface of the contact tube was relatively smooth. Graphite and oxide films reduce contact tube wear. Bits of adhesive bulk material and globular pits were found on the surface. Several cracks existed among the bulk specimens. When the heat input was 6072 J/cm, several parallel furrows and bulk material existed at the inner surface of the contact tube. When the heat input was 9114 J/cm, the contact tube wear was relatively severe. The surface was covered with lots of furrows, adhesive bulks and debris. These furrows were composed of Cu and C. When the heat input was 11,760 J/cm, the contact tube wear was the most severe. Adhesive bulk

materials were observed at the rough surfaces of the contact tube. The main compositions of furrow were Cu, C, O and Fe, which are consistent with the typical features of arc ablation.

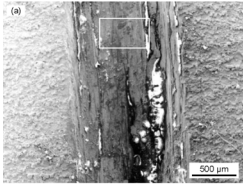
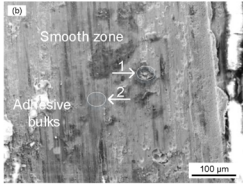
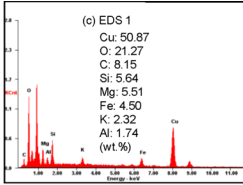
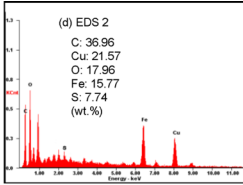
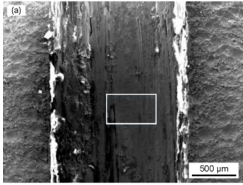
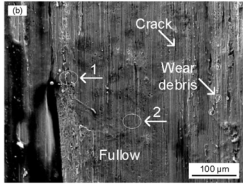
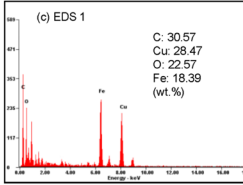
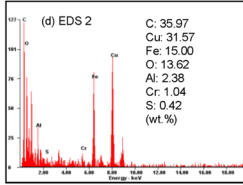
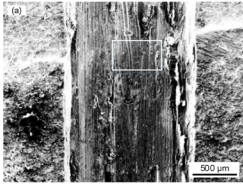
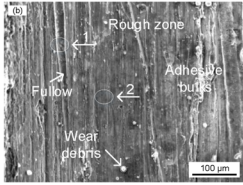
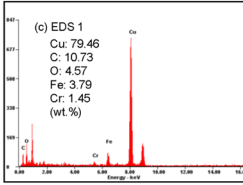
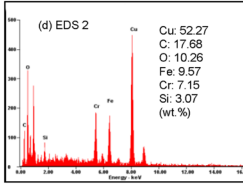
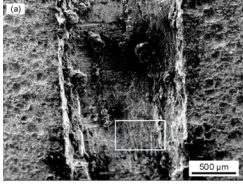
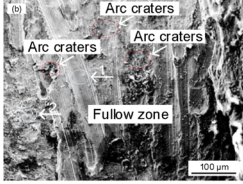
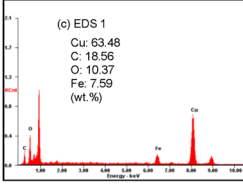
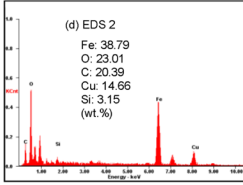
4. Analysis and Discussion

4.1 Effect of Temperature on the Wear Mechanisms of Contact Tube

The contact form includes sliding friction and coating lubrication for the welding wire against the contact tube at room temperature. The contact tube is affected by normal forces and shear forces during the test. With the feeding of welding wires, these forces change dynamically. When the alternating stress increases to a value greater than the endurance limit of the contact tube, fatigue cracks occur and propagate. Some debris is peeled off from the inner surface of the contact tube. These debris are unevenly distributed at the rubbing interfaces. As shown in Table 5, lots of debris were distributed at the cold worn surface of the contact tube for wire C. Some microcracks existed within the bulk materials, demonstrating the typical features of fatigue peeling. Therefore, fatigue peeling is the dominant wear mechanism of the contact tube at room temperature.

As observed in Fig. 4, compared with the cold wear rate, the hot wear rate of the contact tube is slightly increased. When the contact tube temperature is approximately 450 °C, layers of

Table 8 Worn morphology of the contact tube and interface compositions for the wire A under different heat inputs. Test conditions: $I = 150\text{--}350$ A, $U = 20\text{--}36$ V, welding speed = 30–45 cm/min, extension length of wire = 20 mm, DCEP, welding time = 1 h, flow rate of 100% CO₂ shielding gas = 20 L/min

Heat inputs, J/cm	Worn morphology of the contact tube		Microzones compositions of the contact tube	
	Macroscopic worn morphology	Microscopic worn morphology	Point 1 composition	Point 2 composition
4200			 (c) EDS 1 Cu: 50.87 O: 21.27 C: 8.15 Si: 5.64 Mg: 5.51 Fe: 4.50 K: 2.32 Al: 1.74 (wt.%)	 (d) EDS 2 C: 36.96 Cu: 21.57 O: 17.96 Fe: 15.77 S: 7.74 (wt.%)
6072			 (c) EDS 1 C: 30.57 Cu: 28.47 O: 22.57 Fe: 18.39 (wt.%)	 (d) EDS 2 C: 35.97 Cu: 31.57 Fe: 15.00 O: 13.62 Al: 2.38 Cr: 1.04 S: 0.42 (wt.%)
9114			 (c) EDS 1 Cu: 79.46 C: 10.73 O: 4.57 Fe: 3.79 Cr: 1.45 (wt.%)	 (d) EDS 2 Cu: 52.27 C: 17.68 O: 10.26 Fe: 9.57 Cr: 7.15 Si: 3.07 (wt.%)
11760			 (c) EDS 1 Cu: 63.48 C: 18.56 O: 10.37 Fe: 7.59 (wt.%)	 (d) EDS 2 Fe: 38.79 O: 23.01 C: 20.39 Cu: 14.66 Si: 3.15 (wt.%)

oxide films form on the inner surface of the contact tube (Ref 16). These oxide films can avoid the direct contact of the welding wires against the contact tube; thus, the contact tube wear is reduced. The oxide breaks up when the oxide thickness reaches 1 to 3 μm. The oxide becomes debris at the real contact points temperature, thus leading to oxidative wear (Ref 17). When oxidative wear occurs, the contact tube endures severe thermal softening and plastic deformation. In such cases, the wear rate of the contact tube is increased (Ref 18). Based on a theoretical wear rate formula (Ref 19) (formulas 4), the oxidative wear rate of the contact tube (w_T) is proportional to the contact tube temperature (T_c).

$$w_T = \frac{dA_p \exp\left(-\frac{Q_p}{RT_c}\right)}{\xi^2 \rho_0^2 f_0^2 V} A \quad (\text{Eq 4})$$

where w_T is the oxidative wear rate of the contact tube; d is the sliding distances of the wire; A_p is the Arrhenius constant for parabolic oxidation; Q_p is the oxidation activation energy for parabolic oxidation; R is the molar gas constant; T_c is the contact tube temperature; A is total real contact area; ξ is the

thickness of the oxide films; ρ_0 is the density of the oxide films; f_0 is the mass fraction of the oxide films; and V is the feed speed of wire.

Meanwhile, the debris compositions are influenced by the contact tube temperature. Due to the high-temperature oxidation of the debris, the debris is composed of Fe₂O₃ when the contact tube temperature is less than 200 °C. When the contact tube temperature is greater than 200 °C, the debris is composed of Fe₃O₄ (Ref 20). As depicted in Table 5 and Table 6, there was little oxide at the inner surface of the contact tube at 20 °C. This debris was composed of copper. The inner surface of the contact tube at 450 °C was covered with iron oxides. The Fe₃O₄/Fe₂O₃ ratio also increases as the contact tube temperature increases (Ref 21). Fe₃O₄ has a cubic crystalline structure which is easy to shear, so the contact tube wear is reduced. The thinner Fe₂O₃ films are less stable, thus leading to the loss of metal adhesion (Ref 22). In view of the lubricating property of oxides, the lubricating property of Fe₃O₄ outperforms that of Fe₂O₃ (Ref 14). The effect of Fe₂O₃ oxide on the oxidative wear of contact tube is significantly worse than that of Fe₃O₄ oxide.

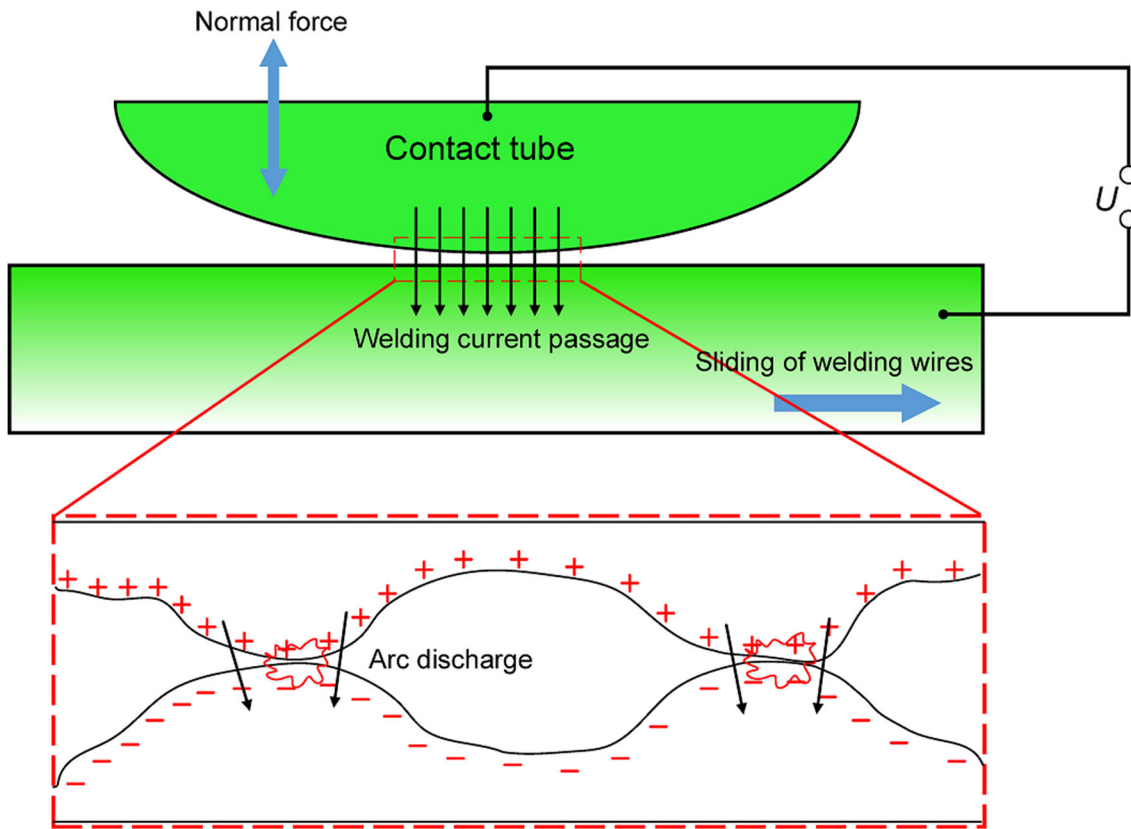


Fig. 7 Mechanism of arc ablation at the rubbing interfaces between the contact tube and the non-copper-coated solid wire when current passes the contact peaks

The hardness of the contact tube surface is mitigated with increasing temperature (Ref 23). The softer inner surface of the contact tube is constantly sheared by the harder microconvex body at the wire surface. The real contact areas are approximately 0.01-0.1% of the apparent areas at the rubbing interfaces. When the distance between two contact peaks is about 1 nm, strong short-range van der Waals forces must be considered. Strong adhesive junctions may be formed at the real area of the contact. These adhesive junctions are sheared and produce bulk particles or wear debris at the inner surface of the contact tube (Ref 24). Adhesive bulk particles and debris covered the inner surface of the contact tube for all wires studied, which demonstrates the typical features of adhesive wear. According to the Archard wear model (Ref 25), the adhesive wear rate of the contact tube is proportional to the load at the contact and is inversely proportional to the hardness of the contact tube. In some degree, the adhesive wear rate of the contact tube is increased with the contact tube temperature.

When there is little lubricant at the rubbing interfaces, the contact tube is constantly sheared by harder microconvex bodies at the wire surface. Meanwhile, the generation rate of furrows is greater than that of the oxide films, causing the oxide films to break up. The debris can be peeled off from the surface layers. In general, some hard particles are embedded into the rubbing interfaces due to several extrinsic factors, thereby forming three-body abrasive wear (Ref 26). These abrasive particles induce high contact stresses between the tribological pairs surface. The inner surface of the contact tube is plastically deformed or fatigued. The furrowing effect of abrasive particles leads to visible grooves. As seen in Table 6, a lot of furrows

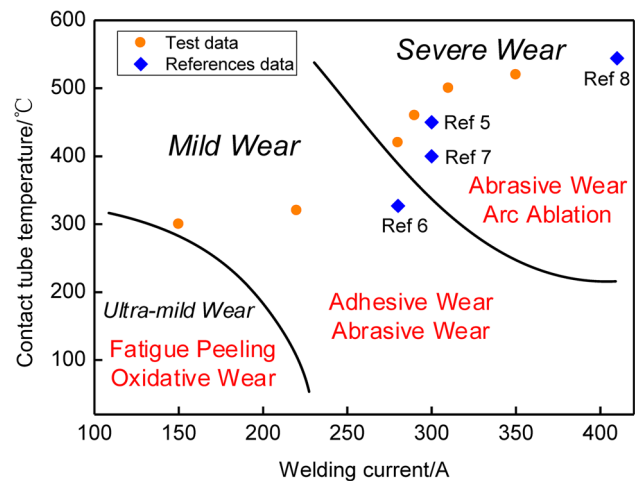


Fig. 8 A wear map of the contact tube for non-copper-coated solid wire at different contact tube temperatures and welding currents

were present at the inner surface of the contact tube for wire C, which demonstrates the typical features of adhesive wear. Consequently, the main wear mechanisms of the contact tube at 450 °C are oxidative wear, adhesive wear and abrasive wear.

The worn morphology of the contact tube for wire B was very severe at the welding conditions. The inner surface of the contact tube for wire B was covered with various furrows. The accumulated debris appeared at the edge of globular pits, which demonstrates the typical features of arc ablation. As depicted in

Table 7, debris and adhesive bulk particles were present on the worn surface of the contact tube for wire A. Therefore, the primary wear mechanisms of the contact tube during welding for non-copper-coated solid wires are abrasive wear and arc ablation. Oxidative wear is the dominant wear mechanism of the contact tube for copper plating wires.

4.2 Effect of Heat Input on Wear Mechanisms of the Contact Tube for Non-copper-Coated Solid Wires

The wear properties of contact tube are directly influenced by the heat input from four respects as follows: 1) the heat radiation from the arc and molten pool; 2) the feeding speed of the wire; 3) the Joule heat of the current generated at the sliding contact; and 4) the arc ablation effect created by the shunting action of the current. The heat effect of the arc is strengthened as the welding current increases. As a result, the peak temperatures of the arc and molten pool escalate. The effect of the heat radiation from arc and molten pool on the contact tube is enhanced, thus the contact tube temperature rises. For CO₂ gas shielded arc welding, the arc peak temperature varies linearly from 1.5×10^4 °C at 100 A to 2.6×10^4 °C at 300 A (Ref 27). The peak temperature of the arc is proportional to the arc length. The effect of heat radiation from the arc on contact tube is raised. For the CO₂ gas shielded arc welding machine, the feeding speed of welding wire is proportional to the welding current. The contact frequency of the wire against the contact tube increases with the current. Fatigue peeling is more distinguished. The amount of debris and bulk particles increases at the inner surface of the contact tube. Therefore, the wear rate of the contact tube is increased. However, with regard to the wear rate of the contact tube during welding, the effect of mechanical friction on the wear properties of the contact tube is limited.

For non-copper-coated solid wires, the contact resistance is approximately 12 mΩ at the sliding contacts. The summation of the Joule heat power is about 216 W (Ref 28). This resistive heat is found to be responsible for the increase of the contact tube temperature. Furthermore, this resistive heat increases rapidly as the welding current increases. The contact tube temperature then rises, which leads to severe oxidation wear. The lubricating effect of the coatings is weakened. The probability of abrasive wear of the contact tube is escalated. In terms of the wear rate of contact tube during welding, however, the effect of the contact tube temperature on the wear properties of contact tube is limited. In such cases, the contact tube temperature rise is generated by the Joule heat of the current and thermal radiation of the arc and molten pool. Consequently, the effect of the heat input on the contact tube is mainly the arc ablation effect. The arc ablation effect is induced by the shunting action of the current.

The contact resistance of the rubbing interfaces is composed of the parallel connection of each contact resistance (Ref 29). The shunting phenomenon of the current appears at the contact peaks. The contact areas and forms of the sliding contacts are continually varied during welding. These observations are due to differences in the current through the contact peaks, based on the differences in the resistance of the contact peaks. Figure 7 shows a sketch of arc ablation at the rubbing interfaces. When the current is relatively high, the gas gap between two contact peaks is broken down into current passage by a strong electric field. Therefore, a gas discharge is created at the rubbing interfaces. Arc discharge is produced at a lower voltage drop

between the contact peaks. Discharge zones emerge at the inner surface of the contact tube (Ref 30). Shearing cracks are induced at the discharge zones because of the effects of normal forces and shear forces. With the sliding of wire, these substances are separated from the contact tube due to fatigue peeling. Simultaneously, the arc heat directly leads to the heat damage of wear debris. These debris accumulate around the arc craters (Ref 31). In addition, the wear rate of the contact tube is approximately linearly correlated with the arc energy. The increase in the normal force can prevent arc discharge and reduce contact tube wear (Ref 32).

The number of arc craters increases with an increase in the heat input. When the current is less than 280 A, the shunting current is low at the contact peaks. The system cannot attain the conditions of arc discharge. In such cases, fatigue peeling, oxidative wear and abrasive wear are the primary wear mechanisms of the contact tube for non-copper-coated solid wires. When the current increases to values greater than 280 A, the shunting current at the contact peaks is high. Arc discharge arises under certain conditions, thereby worsening the state of the contact tube. The dominant wear mechanisms of the contact tube are abrasive wear and arc ablation for non-copper-coated solid wires.

Based on the analysis of different wear mechanisms, a contact tube wear map of non-copper-coated solid wires is established (Fig. 8). The wear map expresses the correlation of the contact tube wear mechanisms with the contact tube temperature and the welding current. The wear map of the contact tube is divided into three zones for non-copper-coated solid wires. The contact tube is transformed from ultra-mild to severe wear in these zones. The primary mechanisms of the contact tube wear are as follows in areas of ultra-mild wear, mild wear and severe wear.

- Fatigue peeling and oxidative wear
- Adhesive wear and abrasive wear
- Abrasive wear and arc ablation

5. Conclusions

- (1) Compared with non-copper-coated solid wires used during welding, the contact tube temperature of the copper plating wire was lower. The wear rate of the contact tube was increased with an increase of the contact tube temperature. The main wear mechanism of the contact tube was fatigue peeling at room temperature. Adhesive wear, oxidative wear and abrasive wear were the dominant wear mechanisms of the contact tube at 450 °C.
- (2) The wear rate of the contact tube during welding was significantly greater than its cold and hot wear rates. The wear rate of the contact tube escalated as the heat input increased for non-copper-coated solid wires. When the heat input was 9114 J/cm, the wear mechanisms of the contact tube were converted from oxidative wear to arc ablation for non-copper-coated solid wire.
- (3) The primary wear mechanisms of the contact tube for non-copper-coated solid wire were fatigue peeling and oxidative wear at the ultra-mild wear zone, adhesive wear and abrasive wear at the mild wear zone, abrasive wear and arc ablation at the severe wear zone.

Acknowledgments

Financial support of the research work by National Natural Science Foundation of China (No. 51574011 and No. 51804196) is gratefully acknowledged.

References

1. S. Goethel, G. Buerkner, and P. Mayr, Alternative Materials for Gas Metal Arc Welding Contact Tubes, *Weld. World*, 2013, **57**, p 879–885
2. O. John and M. Khumbulani, Towards Achieving a Fully Intelligent Robotic Arc Welding: A Review, *Ind. Robot.*, 2015, **42**(5), p 475–484
3. Y.L. Xu, N. Lv, G. Fang, S.F. Du, W.J. Zhao, Z. Ye, and S.B. Chen, Welding Seam Tracking in Robotic Gas Metal Arc Welding, *J. Mater. Process. Technol.*, 2017, **248**, p 18–30
4. E.B. Nunes, N.E. Cavalcante, A.S. Barreto, A.I.N. Silva, and M.F. Motta, Evaluation of the Effect of Heat Input in Superduplex Stainless Steel Deposition by the Plasma Powder Process, *Weld. Int.*, 2016, **31**(3), p 173–183
5. H. Shimizu, Y. Yokota, M. Mizuno, and T. Kurokawa, Wear Mechanism in Contact Tube, *Sci. Technol. Weld. Join.*, 2006, **11**(1), p 94–105
6. H. Shimizu, K. Itoh, N. Masaie, T. Kurokawa, and M. Ushio, Feedability of Wires during Metal Active Gas Welding, *Sci. Technol. Weld. Join.*, 2006, **11**(1), p 81–93
7. J.H. Han, J.J.S. Lee, S.H. Kim, and J.O. Yun, A Study on the Improvement of a Contact Tip for the Wire Melting Rate Enhancement, *Weld. World*, 2017, **61**, p 1181–1187
8. G. Adam, T.A. Siewert, and T.P. Quinn, Contact Tube Temperature during GMAW, *Weld. J.*, 2001, **11**, p 37–41
9. T. Sukru, Tribological Behaviour of Borided Bearing Steels at Elevated Temperatures, *Surf. Coat. Technol.*, 2006, **201**, p 2230–2239
10. A. Senouci, H. Zaidi, and J. Frene, Damage of Surfaces in Sliding Electrical Contact Copper/Steel, *Appl. Surf. Sci.*, 1999, **144**, p 287–291
11. Y.A. Wang, J.X. Li, and Y. Yan, Effect of Electrical Current on Tribological Behavior of Copper-Impregnated Metallized Carbon Against a Cu-Cr-Zr Alloy, *Tribol. Int.*, 2012, **50**, p 26–34
12. S.G. Jia, P. Liu, F.Z. Ren, B.H. Tian, M.S. Zheng, and G.S. Zhou, Sliding Wear Behavior of Copper Alloy Contact Wire Against Copper-Based Strip for High-Speed Electrified Railways, *Wear*, 2007, **262**, p 772–777
13. J.P. Tu, W.X. Qi, Y.Z. Yang, F. Liu, J.T. Zhang, G.Y. Gan, N.Y. Wang, X.B. Zhang, and M.S. Liu, Effect of Aging Treatment on the Electrical Sliding Wear Behavior of Cu-Cr-Zr alloy, *Wear*, 2002, **249**, p 1021–1027
14. Z.X. Li, Q. Wan, G.D. Li, H. Li, H.J. Li, T.L. Zhang, H.J. Kim, and W. Tillmann, Lubrication Mechanisms of C-MoS₂-Fe₂O₃ (Fe₃O₄) Nano-Composite Lubricants at the Rubbing Interfaces of Non-Copper Coated Solid Wires Against the Contact Tube, *Materialwiss. Werkstofftech.*, 2019, **50**, p 52–63
15. M. Grandin and U. Wiklund, Influence of Mechanical and Electrical Load on a Copper/Copper-Graphite Sliding Electrical Contact, *Tribol. Int.*, 2018, **121**, p 1–9
16. A.W. Batchelor, G.W. Stachowiak, and A. Cameron, The Relationship Between Oxide Films and the Wear of Steels, *Wear*, 1986, **113**, p 203–223
17. T.F.J. Quinn, Review of Oxidational Wear Part I: THE Origins of Oxidational Wear, *Tribol. Int.*, 1983, **16**(5), p 257–271
18. Q.Y. Zhang, K.M. Chen, L. Wang, X.H. Cui, and S.Q. Wang, Characteristics of Oxidative Wear and Oxidative Mild Wear, *Tribol. Int.*, 2013, **61**, p 214–223
19. T.F.J. Quinn, Oxidational Wear, *Wear*, 1971, **18**, p 413–419
20. T.F.J. Quinn, D.M. Rowson, and J.L. Sullivan, Application of the Oxidational Theory of Mild Wear to the Sliding Wear of Low Alloy Steel, *Wear*, 1980, **65**, p 1–20
21. S. Hernandez, J. Hardell, C. Courbon, H. Winkelmann, and B. Prakash, High Temperature Friction and Wear Mechanism Map for Tool Steel and Boron Steel Tribopair. *Tribol-Mater. Surf. Int.* 2014, **8**(2), 74–84
22. S.B. Sakrani and J.L. Sullivan, Iron Oxide Films in Tribological Surfaces of Alloy Steel, *Proc. SPIE*, 1998, **3175**, p 175–179
23. L.A. López, G.Y. Perez, F.J. Garcia, and V.H. López, Study of GMAW Process Parameters on the Mechanisms of Wear in Contact Tips C12200 Alloy, *Mater. Res. Soc. Symp. Proc.*, 2015, **1766**, p 53–62
24. R. Aghababaei, D.H. Warner, and J.F. Molinari, On the Debris-Level Origins of Adhesive Wear, *PNAS*, 2017, **114**(30), p 7935–7940
25. J.F. Archard, Contact and Rubbing of Flat Surfaces, *J. Appl. Phys.*, 1953, **24**(8), p 981–988
26. R.I. Trezona, D.N. Allsopp, and I.M. Hutchings, Transitions Between Two-Body and Three-Body Abrasive Wear: Influence of Test Conditions in the Microscale Abrasive Wear Test, *Wear*, 1999, **225–229**, p 205–214
27. J. Hu and H.L. Tsai, Heat and Mass Transfer in Gas Metal Arc Welding. Part I: The Arc, *Int. J. Heat. Mass. Trans.* 2007, **50**, 833–846
28. H. Shimizu, Y. Yokota, T. Itoh, T. Kurokawa, and M. Ushio, Joule Heating of Solid Wires in MAG Welding, *Weld. Int.*, 2005, **19**(10), p 761–772
29. L. Kogut and K. Komvopoulos, Electrical Contact Resistance Theory for Conductive Rough Surfaces, *J. Appl. Phys.*, 2003, **94**(5), p 3153–3162
30. G.X. Xie, D. Guo, and J.B. Luo, Lubrication under Charged Conditions, *Tribol. Int.*, 2015, **84**, p 22–35
31. X.Z. Xiong, C.J. Tu, D. Chen, J.Q. Zhang, and J.H. Chen, Arc Erosion Wear Characteristics and Mechanisms of Pure Carbon Strip Against Copper under Arcing Conditions, *Tribol. Lett.*, 2014, **53**, p 293–301
32. G.X. Chen, H.J. Yang, and W.H. Zhang, Experimental Study on Arc Ablation Occurring in a Contact Strip Rubbing Against a Contact Wire with Electrical Current, *Tribol. Int.*, 2013, **61**, p 88–94

Publisher's Note Springer Nature remains neutral with regard to jurisdictional claims in published maps and institutional affiliations.